

Evidence for an intermediate mass black hole and a multi-zone warm absorber in NGC 4395

D. C. Shih,^{1,2} K. Iwasawa¹ and A. C. Fabian¹

¹ *Institute of Astronomy, Madingley Road, Cambridge, CB3 0HA*

² *Department of Physics, Princeton University, Princeton, NJ 08544*

ABSTRACT

We report on the results of an analysis in the X-ray band of a recent long *ASCA* observation of NGC 4395, the most variable low-luminosity AGN known. A relativistically-broadened iron line at ~ 6.4 keV is clearly resolved in the time-averaged spectrum, with an equivalent width of 310_{-90}^{+70} eV. Time-resolved spectral analysis of the heavily absorbed soft X-ray band confirms the existence of a variable, multi-zone warm absorber in this source, as proposed in a previous analysis of a shorter *ASCA* observation. The light curve of the source is wildly variable on timescales of hours or less, and a factor of nearly 10 change in count-rate was recorded in a period of less than 2000 s. The long observation and variability of the source allowed the power density spectrum (PDS) to be constructed to an unprecedented level of detail. There is evidence for a break in the PDS from a slope of $\alpha \sim 1$ to $\alpha \sim 1.8$ at a frequency of around 3×10^{-4} Hz. The central black hole mass of NGC 4395 is estimated to be approximately 10^4 – $10^5 M_{\odot}$ using the break in the PDS, a result consistent with previous analyses using optical and kinematical techniques.

Key words: galaxies: individual: NGC 4395 – galaxies: Seyfert – X-rays: galaxies.

1 INTRODUCTION

NGC 4395 is a nearby ($d \sim 2.6$ Mpc) dwarf galaxy containing an active nucleus. The nucleus harbors a small black hole of mass less than $8 \times 10^5 M_{\odot}$ (Filippenko & Ho 2003). The optical emission-line spectrum of the nucleus is dominated by non-stellar emission, reminiscent of normal Seyfert galaxies but with a much lower luminosity (Ho et al. 1997). Indeed, NGC 4395 is one of the lowest-luminosity AGN, with an absorption-corrected 2–10 keV luminosity of 4×10^{39} erg s⁻¹. However, in contrast to other low luminosity active nuclei, which are usually found at the centers of galaxies having large bulges and which exhibit weak X-ray variability (Ptak et al. 1998), NGC 4395 has no significant bulge and shows strong X-ray variability. Interestingly, it appears to lie on the anti-correlation between X-ray variability amplitude and luminosity found in higher luminosity Seyfert nuclei (Nandra et al. 1997). In terms of a possible link between black hole mass and X-ray variability, NGC 4395 is therefore of great interest, given the fact that it is one of the few objects containing a small black hole of well-determined mass.

It is a well-established fact that the X-ray light curves of active galaxies show a red-noise characteristic, and approximating the power spectrum with a power law typically gives slopes of 1.5–2 on time scales of hours to days. Evidence for a flattening of the power-law slope on longer time scales, similar to that found in Galactic Black Hole Candidates (GBHC) but scaled to much shorter time

scales, has been found in some active galaxies. Being a low-mass black hole AGN, NGC 4395 provides us with an opportunity to examine the interesting part of the power spectrum with a relatively short monitoring time compared with its higher luminosity counterparts.

In addition to extreme X-ray flux variability, NGC 4395 is also known to exhibit interesting spectral variability as well. The source was previously observed by *ASCA* in 1998, and an analysis by Iwasawa et al. (2000) found the time-averaged X-ray spectrum to be well-described by a power-law continuum with a photon index of 1.5–2, with heavy absorption below ~ 3 keV and marginal evidence for iron line emission at ~ 6.4 keV. During a large flare in the 1998 observation, the spectrum was observed to vary dramatically below 3 keV, with the absorption appearing to lessen considerably between 1–2 keV. A single-zone warm absorber was found to give a physically inconsistent description of the active/quiescent states, and a two-zone warm absorber consisting of a constant and a variable component was proposed to explain the observed spectral variability.

In this paper, we present the results of an analysis of a week-long *ASCA* observation of NGC 4395, focusing on the temporal and spectral variability of the X-ray source. Since the previous observation was only a half-day in duration, the conclusions reached in this analysis represent a significant improvement in our understanding of this source.

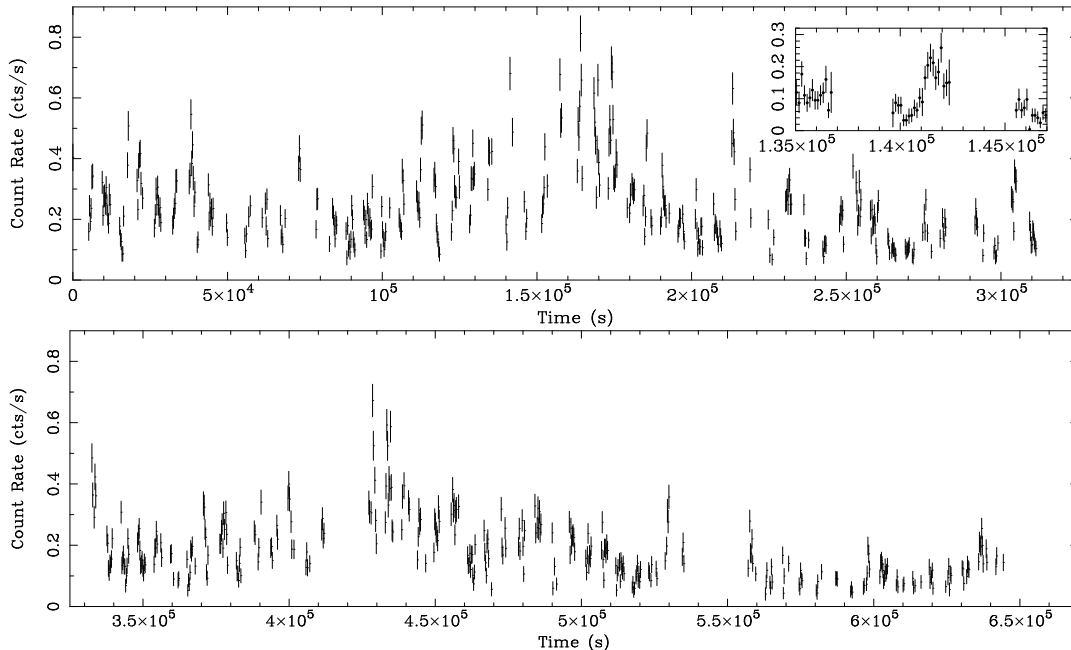


Figure 1. The 1.2–10 keV band SIS+GIS background-subtracted light curve with 256-s time bins. The inset shows (for the SIS0 detector only and with 128-s bins) a particularly fast X-ray variation, with the count rate increasing by a factor of nearly 10 in ~ 1500 s.

2 OBSERVATION AND DATA REDUCTION

NGC 4395 was observed by *ASCA* from 2001 May 25 to 2001 June 1, for a total exposure time of 640 ks. Data reduction was carried out using the method of Iwasawa et al. (2000). Following GTI filtering, the good exposure time was approximately 300 ks for the SIS and 280 ks for the GIS. The mean count rates for the SIS/GIS (using the large-aperture region – see below) were 0.075/0.079 cts/s in the 2–10 keV band and 0.038/0.028 cts/s in the 1–2 keV band. The observed 2–10 keV flux averaged over the whole observation is 4.7×10^{-12} erg cm $^{-2}$ s $^{-1}$, very similar to that obtained from the previous short *ASCA* observation, while the source is highly variable. The time-averaged 1–2 keV flux is 3.1×10^{-13} erg cm $^{-2}$ s $^{-1}$, somewhat higher than the corresponding flux of 2.6×10^{-13} erg cm $^{-2}$ s $^{-1}$ of the previous *ASCA* observation.

Several circumnuclear X-ray sources are known to exist within 10 arcmin of the nucleus of NGC 4395 (Moran et al. 1999; Lira et al. 1999; Iwasawa et al. 2000). In this observation, we could only detect the brightest of these background sources, corresponding to source E of Moran et al. (1999), a very soft source located ~ 2.8 arcmin away from the nucleus, with X-ray emission peaking below 1 keV. We have checked that the mean fluxes from source E and the nucleus in various energy bands are in agreement with the previous *ASCA* observation within 15 per cent, and that source E does not show significant variability. Therefore, we have chosen to use in this analysis the source regions defined by Iwasawa et al. (2000) in their analysis of the previous observation. We briefly describe here the definition of these regions. Since the flux of source E is negligible relative to the nucleus above ~ 2 keV, we use photons collected from a large-aperture (6 arcmin diameter) circular region around the nucleus (but excluding a small 1 arcmin circular region around source E) for analysis above 2 keV. Below 2 keV, the contamination due to source E becomes non-negligible owing to the broad point spread function of the *ASCA* X-ray telescope. In fact it may be as high as 70% in the large-aperture region. To mini-

mize this contamination we use instead a small-aperture (3 arcmin diameter) region around the nucleus for any analysis requiring data below 2 keV (e.g. analysis of the warm absorber) so that the contamination from the source E in the 1–2 keV band should be less than 10 per cent (see Iwasawa et al. 2000).

3 TIMING ANALYSIS

3.1 X-ray Light Curves

The strong X-ray variability of NGC 4395 suggested by the previous short *ASCA* observation is confirmed in this long observation, as can be seen in the light curve shown in Fig. 1. The light curve is the sum of the SIS and GIS light curves and includes background subtraction. Each point represents a full 256-s of good exposure time. The source is seen to vary wildly on timescales of hours or less. In several instances, the count rate was observed to change by nearly an order of magnitude on time scales of ~ 2000 s; the most dramatic example is shown in the inset of Fig. 1.

The energy dependence of the normalized excess variance σ_{rms}^2 (see Nandra et al 1997 for the definition) of the light curve is plotted in Fig. 2. On a wide range of timescales, the strongest variability is found in the 1–2 keV band. As mentioned above, any contamination from source E has little effect on this excess variability in this energy range. The variability of the warm absorber, and not of the primary continuum, is likely to be the main contributor to the peak in the RMS variance spectrum. Indeed, in the context of the multi-zone warm absorber model to be discussed in detail in Section 4.2, we see that the variability in the 1–2 keV band can be attributed to rapid changes in a highly ionized, dense absorber located close to the source.

3.2 The Power Density Spectrum

The power density spectrum (PDS) of NGC 4395 was computed for the 1.2–10 keV band light curve using data from all four detectors following the method of Hayashida et al. (1998). The one difference with the method of Hayashida et al. (1998) was that geometric rather than arithmetic averaging was employed to smooth the PDS. Smoothing the logarithm of the PDS instead of the PDS itself tends to give a less biased estimate of the PDS when the number of points in each frequency bin is small (Papadakis & Lawrence 1993). 5760-s bins were used to obtain the low frequency PDS and 128-s bins to obtain the high frequency PDS. These binsizes were also chosen so as to avoid frequencies around 10^{-4} Hz, where contamination from the orbital period of the spacecraft produces a spurious peak in the PDS. Segments with less than four time bins were not used in the calculation in an attempt to limit the effect of red-noise leak. The low frequency PDS was smoothed with $N = 5$ and the high frequency PDS with $N = 25$.

The result of the calculation using the 1.2–10 keV light curve is shown in Fig. 3. We report a possible detection of a break in the power spectrum. A single power-law with best-fit slope $\alpha = 1.29 \pm 0.04$ gives a relatively poor description of the PDS ($\chi^2 = 37.6$ for 24 degrees of freedom). A broken power-law with $\alpha_1 = 0.98 \pm 0.18$ ($f < f_b$), $\alpha_2 = 1.78 \pm 0.19$ ($f \geq f_b$), and break frequency $f_b = 3.2_{-1.6}^{+3.2} \times 10^{-4}$ Hz gives an improved fit ($\chi^2 = 27.9$ for 22 degrees of freedom). The improvement is significant at a 96% confidence level according to the standard F-test. We note, however, that the F-test is a crude measure of significance and must be interpreted with caution. In particular, it does not take into account systematic biases such as aliasing and red-noise leak which could cause the spurious detection of a break.

The PDS was also calculated using the 2–10 keV light curve to check whether variability of the warm absorber below ~ 2 keV could have a significant effect on the parameters of the measured power spectrum. The broken power law slopes, and more importantly, the *location of the break* measured from the 2–10 keV band PDS agrees within errors with those quoted above. It was noted in Section 3.1 that the RMS variance spectrum peaks in the 1–2 keV band, most likely due to changes in the warm absorber and not the source itself. However, the fact that the break in the PDS is present and has the same frequency (within errors) in both the 1.2–10 keV band and the 2–10 keV band suggests that the break is an intrinsic feature of the source. Indeed, since the shape of the PDS is similar between the bands, the 1.2–10 keV band PDS seems to provide a measure of the intrinsic source variability. The additional effect of the variable warm absorber is undetectable in the PDS owing to its limited bandwidth (1.2–2 keV), the high intrinsic variability of the source, and the large uncertainties of the measured PDS.

The shape of the PDS is remarkably similar to those of Galactic Black Hole Candidates (GBHC) in the low state. The PDS of Cygnus X-1, among the most famous and well-studied GBHC, has been measured to very high accuracy over nearly five decades in frequency in a number of observations (Gilfanov et al. 1999; Nowak et al. 1999; Belloni & Hasinger 1990). It too exhibits a spectral steepening from $\alpha \approx 1$ to $\alpha \approx 1.5$ – 1.7 as one increases in frequency, while at lower frequencies the PDS hits a “knee” and becomes nearly flat. This three-component behavior has also been observed in several other GBHC (e.g. Miyamoto 1992). While a longer observation is needed to test for the presence of a flat component at very low frequencies in the PDS of NGC 4395, the similarity of the two higher-frequency components to the power spec-

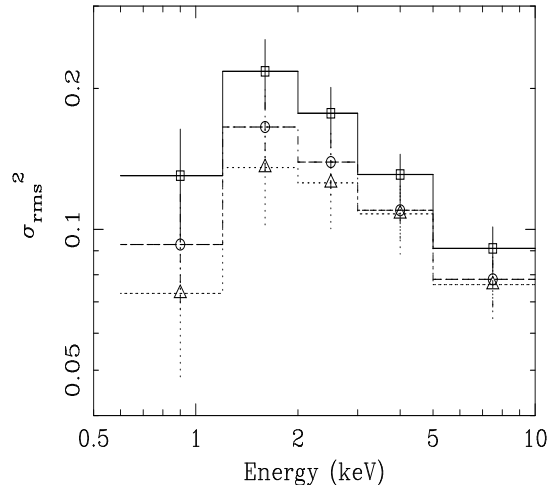


Figure 2. The normalized RMS variance spectrum on 12 ks (squares), 23 ks (circles), and 46 ks (triangles) timescales. The peak in RMS variance in the 1–2 keV band is most likely due to a variable warm absorber, a hypothesis that we shall explore in Section 4.2.

tra of GBHC suggests that the physical processes that give rise to X-ray variability in GBHC are similar to those of NGC 4395. A better understanding of the X-ray variability of the former, enabled by their much higher signal-to-noise and shorter variability time scales, might therefore lead to improved knowledge of NGC 4395.

As a preliminary attempt at a comparison, we can use the striking similarity between the power spectra of NGC 4395 and Cyg X-1 in order to obtain an estimate of the black hole mass of the former, following the scaling method of Hayashida et al. (1998). We shall describe the technique and results in detail in Section 5. Here, we merely note that in the analysis of the previous short *ASCA* observation by Iwasawa et al. (2000), the mass of NGC 4395 was estimated using the PDS to be about $3 \times 10^4 M_{\odot}$. The PDS obtained in that analysis, however, consisted of only a handful of points, and so neither the break frequency nor the slope of the PDS could be measured. Instead, the authors used a template PDS taken from NGC 4051, which breaks from $\alpha = -0.28$ to $\alpha = 2.01$, and scaled it to the PDS of NGC 4395 with the break frequency as a free parameter. With the much more detailed power spectrum from the current observation, we are actually able to both measure the break frequency and the spectral slopes, and we see that in fact the NGC 4051 PDS is a very poor template for NGC 4395.

4 SPECTRAL ANALYSIS

4.1 Time-Averaged Spectrum: Warm Absorber and Iron K α Line

The X-ray spectrum of NGC 4395 is known to be heavily absorbed by what is thought to be ionized material along the line of sight (the so-called warm absorber). With non-negligible absorption extending up to or even beyond 3 keV, the likely presence of a broad iron line around 5–7 keV, a reflection hump from the disk starting at ~ 10 keV, and an iron K edge around 8 keV due to the warm absorber, obtaining a reliable value for the continuum photon index is a highly non-trivial task. Fig. 4 shows the result of a preliminary power-law fit to the SIS in the 3–10 keV continuum band, extrapolated to lower energies. The residuals at ~ 6 keV are highly suggestive of iron-line emission. The extrapolation to lower ener-

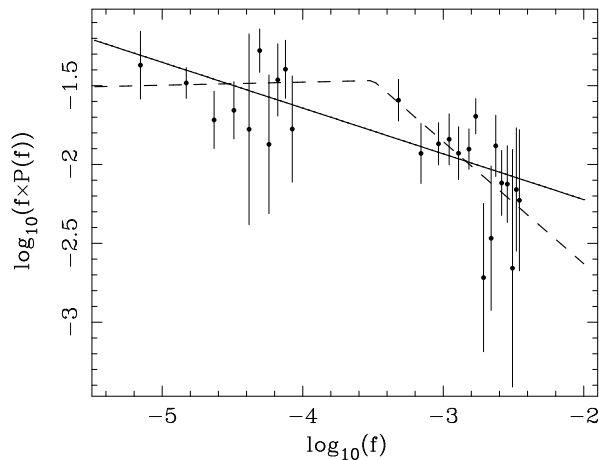


Figure 3. The normalized power density spectrum (NPDS) of NGC 4395 derived from the 1.2–10 keV band light curve, plotted as frequency times power. The solid line shows the best-fit single power law to the entire PDS ($\alpha = 1.29$), while the dashed line shows the best-fit broken power law ($\alpha_1 = 0.98, \alpha_2 = 1.78, f_b = 3.2 \times 10^{-4}$ Hz).

gion reveals the tell-tale signature of warm absorption: a blend of absorption lines and edges due to partially-ionized, obscuring material.

The best-fit photon index for this simple power-law fit was unusually hard, $\Gamma \approx 1$. A hard photon index ($\Gamma \approx 0.6$) was also recently reported by Moran et al. (2001) during a recent 17 ks *Chandra* observation of NGC 4395. The discrepancy between the photon index measured in the present analysis and that of Moran et al. (2001) might be explained by the effects of photon pile-up. The same *Chandra* data analyzed by Moran et al. (2001) were found to be affected by the CCD pile-up (Davis 2001), despite the attempt of reducing it by using faster readout. On the other hand, pile-up should be completely negligible in the *ASCA* data of the present analysis. The point spread function of *ASCA* is far broader than that of *Chandra*, and there is correspondingly very little chance in the *ASCA* data of more than two photons falling into a single pixel within a single readout for a faint source such as NGC 4395. Two important effects of the pile-up are: 1) the light curve has reduced flux peaks where the pile-up occurs; and 2) the spectrum is distorted to have a harder slope than is actually present. The second effect might have resulted in the very small photon index measured by Moran et al. (2001). The range of X-ray flux variations in NGC 4395 is quite large: from very low count rates where the pile-up is negligible to high count rates where significant pile-up occurs. The high-flux state is where the spectral softening due to 1–2 keV flux increase has been found in the two *ASCA* observations (e.g., see Fig. 6). The spectral distortion due to the pile-up would reduce this spectral softening for high flux state if it was not corrected, affecting a spectral variability study. In any case, it is extremely unlikely that these low photon indices are associated with the intrinsic source spectrum, given the standard mechanism of continuum production via inverse-Compton scattering of thermal disk photons off a hot, optically-thin corona (Moran et al. 2001). A more plausible explanation is that the source has an intrinsically steep spectrum, that is then modified, perhaps by obscuring material along the line of sight, to produce a flat spectrum. Moran et al. (2001) suggest that this obscuring material could be due to neutral “partial covering” components. As they note in their paper, however, this partial-covering model predicts a strong Fe K edge near 7 keV that is not

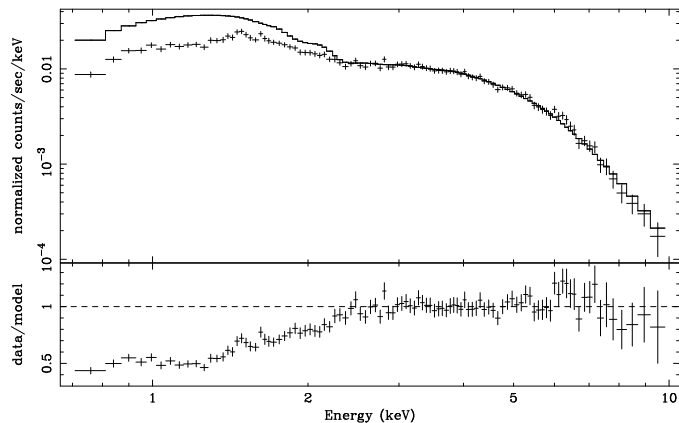


Figure 4. The time-averaged SIS spectrum, along with the best-fit power law to the 3–10 keV band. The ratio of data to model shown in the bottom panel illustrates the heavy absorption below 3 keV, as well as the residuals at ~ 6 keV due to iron-line emission. A moderately strong (EW ~ 300 eV) broad iron line is detected in the present observation at the 99% confidence level.

observed. Below, we will consider another possible explanation for the flatness of the continuum, namely that the (multi-zone) warm absorber is so heavily ionized, that absorption above 3 keV flattens the observed spectrum.

To investigate the residuals at 6 keV, a relativistically broadened 6.4 keV iron line was added to the spectrum using the *diskline* model in *XSPEC* (Fabian et al. 1989). The free parameters were the inclination angle θ_0 and emissivity index α of the accretion disk, and the total line flux $F_{K\alpha}$. The inner and outer radii were frozen at $6 r_g$ and $100 r_g$. In addition, cold absorption was included (with the column density as a free parameter) in order to model the effect of the warm absorber above 2 keV. Since we only expect to see the smooth tails of the ionized warm absorber edges above 2 keV, these can be approximated phenomenologically by the *wabs* neutral absorption model in *XSPEC*. Finally, the effects of neutral reflection by the accretion disk were taken into account by using *pe xrav* instead of a simple power-law for the underlying continuum. The power-law index Γ and overall normalization were left free to vary. The remaining *pe xrav* parameters were frozen at reasonable values: the high-energy cut-off, reflection fraction, and iron abundance were fixed to 200 keV, 1, and $1 Z_\odot$, respectively.

The model was fit to data between 2–10 keV from all four detectors. An acceptable fit was obtained with $\chi^2 = 1431.6/1423$ *dof*, representing an improvement of $\Delta\chi^2 = 16.3$ with three additional parameters over *pe xrav* plus cold absorption alone, and an improvement of $\Delta\chi^2 = 30.2$ with three additional parameters over a power law plus cold absorption alone. The best-fit absorption column density was $1.32^{+0.08}_{-0.18} \times 10^{22}$ cm^{-2} , while the best-fit photon index was $\Gamma = 1.46^{+0.02}_{-0.06}$. The iron-line parameters were well-constrained: $\theta_0 = 49^{+8}_{-4}$ degrees, $\alpha = -2.7^{+0.8}_{-1.0}$, $F_{K\alpha} = 1.4^{+0.3}_{-0.4} \times 10^{-5}$ $\text{ph s}^{-1} \text{cm}^{-2}$ (corresponding to an equivalent width of 310^{+70}_{-90} eV).

We estimate the detection of a broad iron line in NGC 4395 to be significant at the 99% level based on an F-test using a single-gaussian fit to the iron line. The free parameters of the single-gaussian fit were the line energy E_0 and the width σ , as well as the overall normalization. The line width was either frozen at $\sigma \equiv 0$ for a narrow line, or allowed to vary for a broad line. The result of the fits was $\chi^2 = 1436/1424$ *dof* vs. $\chi^2 = 1430/1423$ *dof* for a narrow line vs. a broad line. The best fit line parameters were $E_0 =$

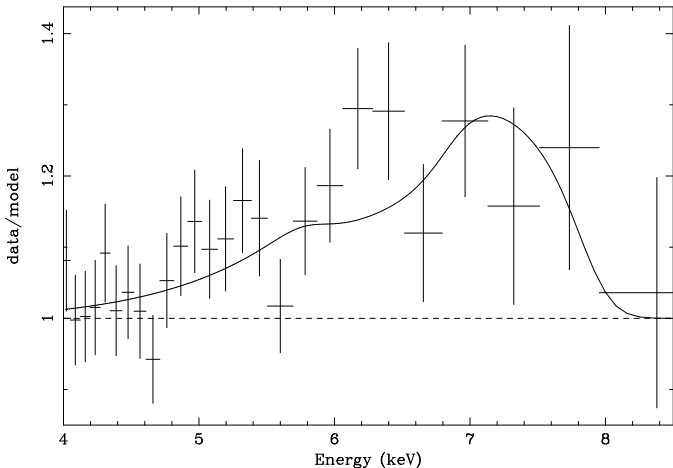


Figure 5. The ratio of the SIS spectrum to the best-fit continuum model. The *diskline* model is shown in the solid line. The excess signifies the clear presence of a broad iron $K\alpha$ line and is described well by the *diskline* model.

$6.32^{+0.07}_{-0.03}$ keV for the narrow line and $E_0 = 6.26 \pm 0.20$ keV, $\sigma = 0.89^{+0.31}_{-0.21}$ eV for the broad line. This significant detection of a broad iron line represents an improvement over the marginal detection in the previous *ASCA* observation of Iwasawa et al. (2000), thanks to the much larger signal-to-noise of this observation. The detected iron line is plotted in Fig. 5 as the ratio of the SIS spectrum to the best-fit continuum model. The strength and broad width of the line is evident.

The spectrum below 4 keV was modeled using a *CLOUDY* v90.04 table model, which describes one-zone, equilibrium, photoionized absorption (Ferland 1991). As mentioned in Section 2, small-aperture spectra were used for the analysis of the warm absorber, so as to minimize contamination due to nearby circumnuclear sources. In order to remain consistent with the continuum fit above 2 keV, the *CLOUDY* photon index was frozen at $\Gamma = 1.46$. The free parameters of the fit were thus the column density and ionization parameter of the warm absorber. The overall χ^2 of the fit was acceptable (256.4/243 degrees of freedom), but obvious trough-like residuals around 1.5–2 keV strongly suggested a more complex pattern of absorption not well-accounted for by *CLOUDY* alone. Also, we will see in Section 4.2 that the single-zone *CLOUDY* model fails to adequately describe the flux-binned spectra. In particular, the pattern of absorption in the low-flux state cannot be modelled using our simple single-zone *CLOUDY* model.

The addition of two absorption edges (the multiplicative edge model in *XSPEC*) did the trick: the residuals were smoothed out, and the individual χ^2 s in the fit to the flux-binned spectra were all good (see Section 4.2). The best-fit parameters for the *CLOUDY* plus edges model are shown in the first row of Table 1. We note that the two extra absorption edges are fairly deep – compare, for instance, with the results of Otani et al. (1996) for MCG–6-30-15. Note also that the inclusion of the two edges is strongly favored by the F-test: a χ^2 of 229.9/239 *dof* with the edges, versus a χ^2 of 256.4/243 *dof* corresponds to an F-test confidence level $> 99\%$. The depth of these edges and the F-test both strongly suggest a more complex picture of ionized absorption than that of the simple single-zone *CLOUDY* model.

A promising alternative is the *multi-zone* warm absorber consisting of two or more partially-ionized, absorbing regions with different physical properties and lying at different posi-

tions along the line of sight. Spectral variability studies have strongly implied the existence of a multi-zone warm absorber in several sources, including MCG–6-30-15 (Otani et al. 1996; Morales et al. 2000), NGC 3516 (Kriss et al. 1996), and recently NGC 4051 (Collinge et al. 2001). In the previous short *ASCA* observation of NGC 4395, a two-zone warm absorber (one constant and less ionized, the other variable and more ionized) was argued for based on an unphysical *decrease* in column density and ionization parameter observed during a flare (Iwasawa et al. 2000).

The result of a two-zone warm absorber fit to the time-averaged spectrum (below 4 keV) is shown in the first row (flux bin 0) of Table 2. The model used was a hybrid *CLOUDY/absori* model, with the former (latter) used to model the constant (variable) component. The ionization parameters and column densities of the two models, along with the underlying photon index, were left free to vary. The temperature of the accretion disk in *absori* was fixed to 10^6 K. The model clearly describes the time-averaged spectrum well. The column density and ionization parameter of the constant component agrees well with the *CLOUDY* plus edges fit described previously (see the first row of Table 1). This gives us confidence in the validity of the arguments above for the necessity of a more complex, multi-zone warm-absorber model. As another consistency check, the column densities of the two zones are in rather good agreement with those obtained in the previous observation (Iwasawa et al. 2000). Meanwhile the ionization parameters, especially of the variable component, are considerably higher than before.

In their recent analysis of a 17 ks *Chandra* observation of NGC 4395, Moran et al. (2001) also find that a two-zone warm absorber model can provide a satisfactory fit to the time-averaged data. However they fix the underlying photon index to $\Gamma = 0.56$, based on a previous *single-zone* warm absorber fit. In our analysis, with our much larger statistical sample, we are able to fit independently for the photon index in the 2–10 keV range with a more sophisticated model consisting of a power-law, reflection, and broad iron line. As a result, we find a much steeper, less exotic photon index of $\Gamma = 1.46$. We are therefore led to a conclusion quite different from that of Moran et al. (2001): NGC 4395 possesses an intrinsically steep power-law continuum with $\Gamma = 1.46$, which is subsequently flattened and modified by multi-zone, ionized absorption, especially around 1.5–2 keV.

A more revealing test of the two-zone warm absorber model is whether it can describe the response of the spectrum to changes in source flux. In the next section, we shall use time-resolved spectral analysis to investigate whether the multi-zone model proposed previously for NGC 4395 can still provide an adequate description of the data, given the higher signal-to-noise and longer exposure time of this observation.

4.2 Time-Resolved Analysis: Multizone Warm Absorber

To investigate the spectral variability of the warm absorber, the data were binned with respect to $F_{1.2-5}$, the SIS0 count rate in the 1.2–5 keV band. Three bins were used, chosen to contain approximately the same number of counts, and defined to be $F_{1.2-5} < 0.025$ cts/s, $0.025 \leq F_{1.2-5} < 0.04$ cts/s, and $F_{1.2-5} \geq 0.04$ cts/s. The bins are numbered 1–3 in order of increasing flux; flux bin 0 denotes the time-averaged spectrum.

The spectral ratios between the data in flux bins 0–3 and the best-fit time-averaged *CLOUDY* plus edges model are plotted in Fig. 6. The model clearly gives a reasonable fit to the time-averaged data, although the residuals still suggest the presence of a com-

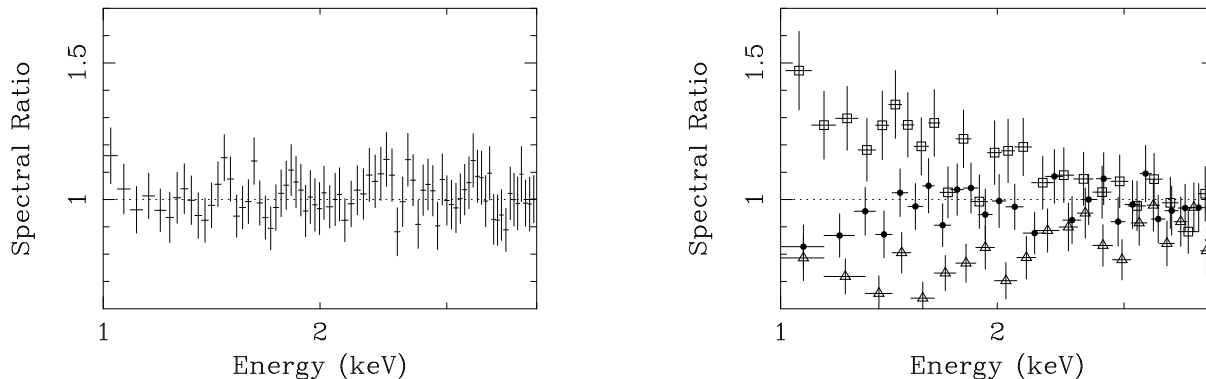


Figure 6. Ratios of the time-averaged spectrum (left panel) and the three flux-binned spectra (right panel) with the time-averaged best-fit model. Open triangles, solid circles, and open squares correspond to flux bins 1–3, respectively. The flux-binned spectra have been renormalized so that the 3–10 keV count-rates agree with the time-averaged spectrum. The absorption clearly lessens as the observed count rate increases. The largest change occurs in the 1–2 keV band, as is expected from the RMS variance spectrum shown in Fig. 2.

Bin	Γ	N_W 10^{22} cm^{-2}	ξ erg cm s^{-1}	E_1 keV	τ_1	E_2 keV	τ_2	χ^2/dof
0	1.46	$2.51^{+0.26}_{-0.28}$	203^{+60}_{-56}	$1.614^{+0.062}_{-0.062}$	$0.153^{+0.058}_{-0.060}$	$1.890^{+0.073}_{-0.067}$	$0.134^{+0.057}_{-0.061}$	229.9/239
1	1.46	$2.24^{+0.34}_{-0.22}$	121^{+47}_{-21}	$1.405^{+0.058}_{-0.053}$	$0.429^{+0.112}_{-0.093}$	$1.857^{+0.066}_{-0.053}$	$0.250^{+0.093}_{-0.088}$	94.6/85
2	—	—	133^{+53}_{-23}	—	$0.009^{+0.092}_{-0.009}$	—	$0.235^{+0.077}_{-0.074}$	95.1/101
3	—	—	220^{+130}_{-49}	—	< 0.060	—	$0.168^{+0.078}_{-0.091}$	81.2/94

Table 1. The best-fit parameters for the CLOUDY plus two edge model fitted to the 1–4 keV spectrum in each flux bin. Flux bin 0 corresponds to the time-averaged spectrum. Errors here and elsewhere are $1\text{-}\sigma$ unless otherwise stated. The dashes indicate that the corresponding parameter has been tied between flux bins.

plex of weak absorption edges (and possibly emission lines) that our simple two extra edges fail to take into account. In flux bins 1–3, the 3–10 keV count rates have been renormalized to that of the time-averaged spectrum. Since the 3–10 keV count rate should be largely unaffected by absorption, the renormalized ratios plotted here should give at least an approximate idea of the variation in absorption. From the plots, it is clear that the warm absorber is changing dramatically with flux. In the low flux bin (bin 1), the spectral ratio reveals a shape characteristic of one or more absorption edges. As we increase in flux, the warm absorber appears to decrease in strength, suggesting that the elements responsible for it are being pushed to higher ionization states due to the increased amount of incident radiation.

We can confirm this interpretation by fitting the CLOUDY plus edge model to the flux-binned spectra. The photon index, being poorly-constrained, was fixed to the best-fit value of the time-averaged 2–10 keV spectrum. The CLOUDY column density and the threshold energies of the edges were tied between the flux-binned spectra. The result of the fits are shown in rows 2–4 of Table 1. The χ^2 is clearly acceptable in the individual flux bins. Also, as mentioned in Section 4.1, the two additional edges are necessary in order to obtain a good fit in the first flux bin. Redoing the fit with CLOUDY alone results in χ^2 s of 118.8/89, 107.3/103, and 85.8/96 *dof* in flux bins 1–3, respectively. Comparing with the χ^2 column in Table 1, we see that two additional edges have a very significant impact on the low-flux bin. The fits confirm the existence of a constant underlying warm-absorber component – while intriguing, the increase in ionization parameter ξ from the second to the third flux bin is not statistically significant. The spectral variation across

flux bins observed in Fig. 6 is primarily accounted for by changes in the optical depths of the photoionization edges. We therefore make the obvious identification of the constant and variable warm absorber with the parameters of CLOUDY and of the extra edges, respectively.

The two-zone warm absorber model confirms this identification. Fits using the CLOUDY/absori model described in Section 4.1 were performed with the column densities of the constant and variable components frozen tied between the flux bins. The results are shown in rows 2–4 of Table 2. The two-zone model describes well the spectral variation with flux, and the variable component behaves in the expected manner, increasing in ionization parameter with increasing source flux. There is strong evidence, therefore, in favor of the two-zone warm absorber model proposed for NGC 4395 by Iwasawa et al. (2000). Absorption around 1.5–2 keV implies that the variable zone is, on average, highly ionized. Depending on the ionization state of the zone, the dominant absorption at these energies should be due to He/H-like Mg and Si. We should note that the high ionization of the variable absorber in all flux states provides an *a posteriori* justification for our model consisting of simple multiplication of the two absorbers (CLOUDY \times absori). This is fortunate, since the proper approach – in which the output from the inner absorber is used as the input for the outer one – would have proved much more difficult.

Perhaps it is also worthwhile to note that the slight increase in the ionization parameter of the constant component (ξ_c) from the second to the third bin persists in the CLOUDY/absori fit. But again it is not statistically significant. In spite of this, it is still very interesting that the ionization parameter of the variable component

Bin	Γ	N_{W}^{c} 10^{22} cm^{-2}	ξ^{c} erg cm s^{-1}	N_{W}^{v} 10^{22} cm^{-2}	ξ^{v} erg cm s^{-1}	χ^2/dof
0	1.46	$2.45^{+0.25}_{-0.32}$	200^{+55}_{-60}	$7.99^{+3.33}_{-2.45}$	481^{+123}_{-111}	232.8/241
1	1.46	$1.91^{+0.31}_{-0.21}$	106^{+26}_{-8}	$5.80^{+0.63}_{-1.23}$	157^{+15}_{-13}	99.2/87
2	—	—	103^{+16}_{-4}	—	436^{+100}_{-83}	96.5/102
3	—	—	159^{+27}_{-16}	—	461^{+85}_{-88}	80.6/95

Table 2. The best-fit parameters for the two-zone CLOUDY plus `absori` model. The “c” and “v” superscripts denote the constant and the variable warm absorber zones, respectively. The dashes indicate that the corresponding parameter has been tied between flux bins.

(ξ_{v}) seems to level off in the high-flux state. Combining this fact with the slight increase in ξ_{c} leads us to suggest the following interpretation of the flux-binned fit: the variable component, assumed to be closer to the nuclear source, becomes completely ionized, and therefore transparent, in the high-flux state. As a result, the constant outer absorber begins to be ionized, and its ionization parameter increases.

A more detailed interpretation of our results and a more general discussion of the warm absorber in NGC 4395 would be too extensive to include in this paper. We should point out that some of the properties of a warm absorber in a small black hole, low luminosity system such as NGC4395 are expected to differ from those in ordinary Seyferts. For instance, the variability time scale of a warm absorber around a normal Seyfert is typically months to years, if the ionized gas is coming from the inner edge of a torus around 1 pc (Kriss & Krolik 2001). On the other hand, 10^3 -s variability in the warm absorber of NGC 4395 is entirely possible, given the low luminosity and high ionization parameter of this source. The properties of warm absorbers in low-luminosity systems such as NGC 4395 is an interesting topic in its own right, and we postpone a more complete discussion to a future publication.

5 DISCUSSION: ESTIMATING THE BLACK HOLE MASS

The break in the power spectrum from $\alpha \sim 1$ to $\alpha \sim 1.8$ at 3.2×10^{-4} Hz found in Section 3.2 gives us a characteristic variability timescale for NGC 4395. Assuming that the variability timescale of a source scales roughly with its size (i.e. a larger source has a longer variability timescale), we can use the measured break frequency and the PDS of a more well-studied source such as Cyg X-1 to obtain an estimate of the black hole mass of NGC 4395. This method has been previously applied to several AGN (e.g. Nowak et al. 2000, Hayashida et al. 1998, Iwasawa et al. 2000), and tends to give mass estimates lower (by as much as 1 or 2 orders of magnitude in some cases) than those obtained from other methods such as X-ray variability, emission line broadening, and modeling the big blue bump (Hayashida et al. 1998).

The $\alpha \sim 1$ to $\alpha \sim 1.8$ break frequency of Cyg X-1 is known to fluctuate between 1–10 Hz (Belloni & Hasinger 1990) over time. The mass of Cyg X-1 is estimated to be $\sim 10 M_{\odot}$ (Herrero et al. 1995). Therefore, if the break frequency scales with the size of the system, we estimate the mass of NGC 4395 to be $M_{\text{BH}} \sim 10^4 - 10^5 M_{\odot}$. This is at the high end of the hard upper limit of $M_{\text{BH}} \lesssim 8 \times 10^5 M_{\odot}$ obtained in recent kinematical studies by Filippenko et al. (2002); but it is encouraging that it is in complete agreement with their “most probable” range.

We can also compare the PDS of NGC 4395 with those of other AGN which have independent, accurate mass measurements. Perhaps the best example of an AGN with a well-determined power spectrum and mass is NGC 5548. Reverberation mapping and kinematical studies of NGC 5548 give a central black hole mass of $(6.8 \pm 2.1) \times 10^7 M_{\odot}$ (Peterson & Wandel 1999), and the PDS agrees with that of Cyg X-1 with a frequency scale factor of $\sim 10^5 - 10^6$ (Chiang et al. 2000). Using NGC 5548 as a template would therefore imply $M_{\text{BH}} \sim 10^5 M_{\odot}$ in NGC 4395, in agreement (albeit at the high end) with the estimate using Cyg X-1.

NGC 4395 is a bulgeless dwarf galaxy (or with a very faint bulge of late spiral). Based on a study of M33, a nearby bulgeless galaxy, Gebhardt et al. (2001) suggest that no supermassive black hole is present in a galaxy with no bulge. They pointed out that a black hole of $100 M_{\odot}$ is sufficient for the luminosity of the active nucleus of NGC 4395 if it is operating at the Eddington limit. The bulge luminosity of NGC 4395 is indeed very low ($M_{\text{B,bulge}} = -10.36$, Ho et al 1997), similar to that of the nucleus of M33, indicating that the black hole driving the active nucleus of NGC 4395 could be as small as $100 M_{\odot}$. However, while there is an order of magnitude uncertainty in our estimate, the X-ray variability results appear to favor the black hole mass to be much larger. The estimates using the optical emission-line properties have also given similar results (Lira et al 1999; Kraemer et al 1999). We also point out that considerable obscuration to the nucleus of NGC 4395, as revealed by hard X-ray observations, leads to the true (optical) nuclear luminosity being underestimated. With a modest bolometric correction ($L_{\text{bol}}/L_{2-10\text{keV}} = 10$), the mean absorption-corrected 2–10 keV luminosity of $4 \times 10^{39} \text{ erg s}^{-1}$ requires a black hole of $\simeq 300 M_{\odot}$ operating at the Eddington limit. The observed light curve shows that the X-ray flux occasionally reaches 6 times higher than the mean value, which implies an even heavier black hole of $\simeq 2 \times 10^3 M_{\odot}$. Moreover, the fact that Seyfert galaxies usually operate at a fraction (a few per cent) of their Eddington luminosity points to that the black hole in NGC4395 might in fact be as large as $10^4 - 10^5 M_{\odot}$. Therefore, either NGC 4395 might be peculiar in that it has a supermassive black hole at the center despite the lack of a significant bulge, or the X-ray source in NGC 4395 exhibits variability in a way which apparently does not scale by the black hole mass.

ACKNOWLEDGMENTS

We thank Simon Vaughan for insights into the subtleties of PDS and timing analysis, Raquel Morales for useful discussions regarding the multi-zone warm absorber and Luis Ho for information on their unpublished result on the black hole mass of NGC 4395. For

support, we thank the Herchel Smith Fellowship (DCS), PPARC (KI), and the Royal Society (ACF).

REFERENCES

- Belloni T. & Hasinger G., 1990, *A&A*, 227, L33.
- Chiang J., Reynolds C. S., Blaes O. M., Nowak M. A., Murray N., Madejski G., Marshall H. L. & Magdziarz P., 2000, *ApJ*, 528, 292.
- Collinge M. J., Brandt W. N., Kaspi S., Crenshaw D. M., Elvis M., Kraemer S. B., Reynolds C. S., Sambruna R. M. & Wills B. J., 2001, *ApJ*, 557, 2.
- Davis J.E., 2001, *ApJ*, 562, 575
- Done C. & Krolik J. H., 1996, *ApJ*, 463, 144.
- Done C., Mulchaey J. S., Mushotzky R. F. & Arnaud K. A. 1992, *ApJ*, 395, 275.
- Fabian A. C., Rees M. J., Stella L. & White N. E., 1989, *MNRAS*, 238, 729.
- Ferland, G. L., 1991, OSU Astronomy Dept., Internal Report 91-01.
- Filippenko A. V. & Ho L. C., 2003, *ApJ*, submitted.
- Gebhardt K., Lauer T. R., Kormendy J., Pinkney J., Bower G. A., Green R., Gull T., Hutchings J. B., Kaiser M. E., Nelson C. H., Richstone D. & Weistrop D., 2001, *AJ*, 122, 2469.
- Gilfanov M., Churazov E. & Revnivtsev M., 1999, *A&A*, 352, 182.
- Hayashida K., Miyamoto S., Kitamoto S., & Negoro H., 1998, *ApJ*, 500, 642.
- Herrero A., Kudritzki R. P., Gabler R., Vilchez J. M. & Gabler A., 1995, *A&A*, 297, 556.
- Ho L. C., Filippenko A. V. & Sargent W. L. W., 1997, *ApJ Supp. Ser.*, 112, 315.
- Iwasawa K., Fabian A. C., Almaini O., Lira P., Lawrence A., Hayashida K. & Inoue H., 2000, *MNRAS*, 318, 879.
- Kraemer S. B., Ho L. C., Crenshaw D. M., Shields J. C. & Filippenko A. V., 1999, *ApJ*, 520, 564.
- Kriss, G. A. & Krolik J. H., 2001, *ApJ*, 561, 684.
- Kriss, G. A., Krolik J. H., Otani C., Espey B. R., Turner T. J., Kii T., Tsvetanov Z., Takahashi T., Davidsen A. F., Tashiro M., Zheng W., Murakami S., Petre R. & Mihara T., 1996, *ApJ*, 467, 629.
- Lira P., Lawrence A., O'Brien P., Johnson R. A., Terlevich R. & Bannister N., 1999, *MNRAS*, 305, 109.
- Lomb N. R., 1976, *Astrophys. & Sp. Sci.*, 39, 447.
- Magorrian J., Tremaine S., Richstone D., Bender R., Bower G., Dressler A., Faber S. M., Gebhardt K., Green R., Grillmair C., Kormendy J. & Lauer T., 1998, *ApJ*, 115, 2285.
- Miyamoto S., Kitamoto S., Iga S., Negoro H. & Terada K., 1992, *ApJ*, 391, L21.
- Morales R., Fabian A. C. & Reynolds C. S., 2000, *MNRAS*, 315, 149.
- Moran E. C., Eracleous M., Leighly K. M., Chartas G., Filippenko A. V., Ho L. C., Blanco P. R., 2001, *astro-ph/0111472*.
- Moran E. C., Filippenko A. V., Ho L. C., Shields J. C., Belloni T., Comastri A., Snowden S. L. & Sramek R. A., 1999, *PASP*, 111, 801.
- Nandra K., George I. M., Mushotzky R. F., Turner T. J. & Yaqoob T., 1997, *ApJ*, 476, 70.
- Nowak M. A. & Chiang J., 2000, *ApJ*, 531, L13.
- Nowak M. A., Vaughan B. A., Wilms J., Dove J. B. & Begelman M. C., 1999, *ApJ*, 510, 874.
- Otani C., Kii T., Reynolds C. S., Fabian A. C., Iwasawa K., Hayashida K., Inoue H., Kunieda H., Makino F., Matsuoka M. & Tanaka Y., 1996, *PASJ*, 48, 211.
- Papadakis I. E. & Lawrence A., 1993, *MNRAS*, 261, 612.
- Peterson B. M. & Wandel A., 1999, *ApJ*, 521, L95.
- Ptak A., Yaqoob T., Mushotzky R., Serlemitsos P. & Griffiths R., 1998, *ApJ*, 501, L37.
- Scargle J. D., 1982, *ApJ*, 263, 835.